Applied and Environmental Microbiology, Jan. 2007, p. 40–47 Vol. 73, No. 1
0099-2240/07/$08.00+0 doi:10.1128/AEM.01442-06
Copyright © 2007, American Society for Microbiology. All Rights Reserved.

Vertical Distribution of Denitrification in an Estuarine Sediment: Integrating Sediment Flowthrough Reactor Experiments and Microprofiling via Reactive Transport Modeling▽

Anniet M. Laverman,[1]* Christof Meile,[2] Philippe Van Cappellen,[1] and Elze B. A. Wieringa[3]

Department of Earth Sciences-Geochemistry, Utrecht University, Utrecht, The Netherlands[1]; Department of Marine Sciences, University of Georgia, Athens, Georgia[2]; and Max Planck Institute for Marine Microbiology, Bremen, Germany[3]

Received 22 June 2006/Accepted 13 October 2006

Denitrifying activity in a sediment from the freshwater part of a polluted estuary in northwest Europe was quantified using two independent approaches. High-resolution N_2O microprofiles were recorded in sediment cores to which acetylene was added to the overlying water and injected laterally into the sediment. The vertical distribution of the rate of denitrification supported by nitrate uptake from the overlying water was then derived from the time series N_2O concentration profiles. The rates obtained for the core incubations were compared to the rates predicted by a forward reactive transport model, which included rate expression for denitrification calibrated with potential rate measurements obtained in flowthrough reactors containing undisturbed, 1-cm-thick sediment slices. The two approaches yielded comparable rate profiles, with a near-surface, 2- to 3-mm narrow zone of denitrification and maximum in situ rates on the order of 200 to 300 nmol cm^{-3} h^{-1}. The maximum in situ rates were about twofold lower than the maximum potential rate for the 0- to 1-cm depth interval of the sediment, indicating that in situ denitrification was nitrate limited. The experimentally and model-derived rates of denitrification implied that there was nitrate uptake by the sediment at a rate that was on the order of 50 (± 10) nmol cm^{-2} h^{-1}, which agreed well with direct nitrate flux measurements for core incubations. Reactive transport model calculations showed that benthic uptake of nitrate at the site is particularly sensitive to the nitrate concentration in the overlying water and the maximum potential rate of denitrification in the sediment.

Anthropogenic inputs of nitrogen are a major cause of eutrophication in aquatic environments (39). Denitrification, the bacterial dissimilatory reduction of nitrate to gaseous products, counteracts eutrophication by removing inorganic nitrogen and releasing it to the atmosphere and by decomposing organic matter (34). The emissions resulting from denitrification, however, include nitrous oxide, a powerful greenhouse gas (8). Because of its environmental importance, denitrification has been the subject of numerous studies (for reviews, see references 12, 16, and 34). Oxygen and nitrate concentrations, temperature, pH, and the availability of suitable electron donor substrates (mainly organic carbon compounds) are considered the key factors controlling the occurrence and rate of denitrification (6, 22, 38).

In estuarine and coastal environments, the most intense denitrification often occurs in sediments, where reduced solute transport rates enable the establishment of anaerobic conditions. A number of methods have been developed to quantify denitrification and related nitrogen transformations in sediments; these methods include, among others, benthic flux measurement (17), isotope pairing techniques (32), and microprofiling using nitrous oxide (31) or nitrate microsensors (9, 20). The available data show that there are large spatial and temporal variations in denitrification rates in nearshore sediments. Ideally, kinetic models of denitrification should account for these variations.

In this study, we combined potential denitrification rate measurements, N_2O microprofiling in acetylene block core incubations, and reactive transport modeling to quantify the depth distribution of the rate of denitrification in a sediment from the freshwater part of a macrotidal estuary. By combining the various approaches, we were able to verify the predictive capability of the kinetic description of denitrification incorporated into the reactive transport model and to assess the sensitivity of benthic nitrate removal to changes in key model parameters.

MATERIALS AND METHODS

Site description. Sediment cores were collected in August 2001 and August 2002 at an unvegetated intertidal site in the freshwater part of the Scheldt Estuary near Appels, Belgium. The Scheldt River has a total length of 355 km and flows through France, Belgium, and The Netherlands. The average river discharge is on the order of 120 m^3 s^{-1}, while the tidal amplitude in the estuary ranges from 2 to 5 m (3). The Scheldt Estuary is heavily polluted by municipal and industrial discharge and intensive livestock farming. The large input of organic matter sustains high heterotrophic activity in the upper freshwater part of the estuary, which can result in a pronounced oxygen depletion zone extending over a distance of 30 to 70 km (42). Intertidal sediments are the primary site of benthic carbon mineralization in the Scheldt Estuary (36). A detailed description of the site is provided elsewhere (13). All cores used in the experiments described here were collected close to each other (<1 m).

Core incubations. Sediment was sampled in August 2002 at low tide using Perspex (acrylic glass) cores with a diameter of 7.6 cm and length of 35 cm. To determine the benthic NO_3^- flux, two cores containing about 20 cm of sediment collected in August 2002 were incubated for 22 h with river water from the site. The overlying water was gently stirred and sparged with air to avoid development of anoxia. The overlying water of the cores was sampled periodically and ana-

* Corresponding author. Mailing address: Department of Earth Sciences-Geochemistry, Utrecht University, P.O. Box 80021, 3508 TA Utrecht, The Netherlands. Phone: 31 30 2536220. Fax: 31 30 2535302. E-mail: anniet@geo.uu.nl.

▽ Published ahead of print on 27 October 2006.

Downloaded from http://aem.asm.org/ on December 8, 2020 at MAX-PLANCK-INSTITUT FUR

lyzed to determine the NO_3^- content. The time-averaged nitrate fluxes into the sediment were calculated from the concentration differences measured in the overlying water between the start and end of the incubations, taking into account the known area of the sediment and volume of overlying water.

To assess pore water transport, three additional cores were incubated with 200 ml NaBr-amended river water from the site. The initial bromide concentrations in the overlying water after NaBr addition were on the order of 10 mmol liter^{-1}. The cores were incubated for 36 h. At the end of the incubation, one core was sectioned into 0.5-cm depth intervals, and the two other cores were sectioned into 1-cm intervals. Pore water was separated from the sediment slices by centrifugation (30 min at 1,000 $\times$ *g*) and filtration (0.45-μm-pore-size Whatman filters) and stored at −20°C until it was analyzed to determine the bromide content. Overlying water samples were collected at the beginning and end of the incubations and analyzed to determine the Br^- concentrations.

Flowthrough reactors. Undisturbed, 1-cm-thick sediment slices were collected in August 2002 with a specially designed hand-held corer. Potential nitrate reduction rates were determined with slices corresponding to depth intervals of 0 to 1, 1 to 2, and 2 to 3 cm using flowthrough reactors (FTRs). The corer, coring technique, FTR design, and potential rate determinations are described in detail elsewhere (18, 25). The reactors were supplied with deaerated inflow solutions containing variable nitrate concentrations (2.5, 5, 7.5, and 10 mmol liter^{-1}; four reactors per depth interval) at a flow rate of 4 ml h^{-1}. Steady-state nitrate reduction rates (R_{exp}) (in nmol cm^{-3} h^{-1}) were calculated after the nitrate concentration in the outflow reached a constant value, as described elsewhere (18). The nitrate reduction rates were fitted to the Michaelis-Menten rate expression:

$$R_{exp} = \frac{R_{max} \cdot [NO_3^-]}{K_m + [NO_3^-]} \quad (1)$$

where K_m is the nitrate half-saturation constant and R_{max} is the maximum nitrate reduction rate. The average nitrate concentration in the reactor ($[NO_3^-]$) was estimated to be the midpoint between the inflow and outflow concentrations. The half-saturation constant was assigned a value of 250 μmol liter^{-1}, the average value derived from a large set of FTR experiments with estuarine sediments, which included additional sampling locations, sampling times, and depth intervals (18).

Microprofiling. Perspex (acrylic glass) cores with a diameter of 4.2 cm and a length of 15 cm were collected at low tide in August 2001 and August 2002. The cores contained about 10 cm of sediment and were incubated at 25°C with river water from the site. The overlying water was gently mixed and sparged with air. Microprofiling was started within 4 h after the cores were collected. Oxygen microprofiles were determined using a miniaturized Clark-type oxygen sensor with an internal reference and a guard cathode (11, 30). Nitrous oxide profiles were determined with a miniaturized Clark-type nitrous oxide sensor with an internal reference and a guard cathode equipped with an oxygen front guard, making it insensitive to oxygen (Unisense, Århus, Denmark). Microprofiles of nitrate were determined only in August 2002, using a Liquid Ion eXchange-type (LIX) electrode (see reference 9) with a calomel reference electrode (Radiometer Copenhagen) and calibrated at the in situ temperature (25°C) and salinity (0‰). Linear two-point calibration of the oxygen and nitrous oxide microsensors was performed with river water from the sampling site. The microelectrodes were mounted on a micromanipulator driven by a computer-controlled motor, making it possible to simultaneously measure vertical distributions of oxygen, nitrate, and nitrous oxide.

Acetylene block experiments. Conversion of N_2O to N_2 and nitrification were inhibited in sediment cores collected in August 2001 and August 2002 by lateral injection of acetylene-saturated water through silicone-filled holes positioned vertically along the core liner. The holes were positioned every 0.5 cm from the sediment surface to a sediment depth of 5 cm. The injections resulted in a C_2H_2 pore water concentration of 10% (vol/vol). Acetylene-saturated river water from the site was added to the core to obtain a final C_2H_2 concentration of 10% (vol/vol) in the overlying water. After addition of C_2H_2, N_2O profiles were recorded with a depth resolution of 250 μm until 2 cm below the sediment surface. Two to eight profiles were recorded sequentially, approximately every 15 min. Ambient oxygen, nitrous oxide, and nitrate (August 2002 cores only) profiles were determined for sediment cores without C_2H_2 addition to determine background N_2O values and check for matrix effects on the sensor readings.

Additional sediment cores collected in August 2001 and August 2002 were supplied with both nitrate and acetylene. One milliliter of a 10-mmol liter^{-1} KNO_3 solution saturated with C_2H_2 was injected laterally into each hole along the core liner, producing pore water NO_3^- concentrations of ~1.7 mmol liter^{-1}. Nitrate was also added to the overlying, acetylene-saturated water to a final concentration of ~2 mmol liter^{-1} (compared to ambient concentrations on the order of 200 μmol liter^{-1}). Time series microprofiles of N_2O were recorded as described above.

Analytical methods. Nitrate, nitrite, and ammonium concentrations were determined colorimetrically with a Nutrient Autoanalyzer 3 (Bran and Luebbe), using standard procedures. Bromide concentrations were determined by ion chromatography (IC Waters, Milford MA). Porosity was determined from the weight loss of a core section having a known volume after oven drying at 105°C. Sediment organic C and total N contents were determined with a Carlo Erba CN analyzer. Inorganic C was removed before the analysis by shaking the sample with 1 mol liter^{-1} HCl twice (12 h and 4 h). Grain size analyses of the bulk sediments were carried out with a Malvern Instruments Mastersizer S. The most probable numbers of denitrifying organisms were determined as described elsewhere (18). Most of the sediment properties reported below were determined using sediment sampled in August 2002; the exceptions were grain size and organic C and total N concentrations, which were determined using sediment collected in May 2002.

Reactive transport modeling. Model calculations were carried out with the Biogeochemical Reaction Network Simulator, a flexible modeling environment for reactive transport calculations (1, 28; http://www.geo.uu.nl/~rtm/index). The time-dependent depth profiles of the concentrations of NO_3^- and N_2O plus the denitrification rate were described by the non-steady-state mass conservation equation for a pore water solute species (2):

$$\frac{\partial C(x,t)}{\partial t} = D_s \frac{\partial^2 C(x,t)}{\partial x^2} + \alpha(x)[C_0(t) - C(x,t)] + R(x,t) \quad (2)$$

where x is the depth in the sediment, t is time, C is the concentration of the solute, C_0 is the solute concentration at the sediment-water interface (SWI), D_s is the in situ molecular diffusion coefficient of the solute corrected for tortuosity (5), α is the nonlocal exchange coefficient, and R is the net rate of production of the solute. At 25°C, 0‰ salinity, and a porosity of 0.80, the D_s values were 2.10 $\times$ 10^{-5} and 1.92 $\times$ 10^{-5} cm^2 s^{-1} for nitrous oxide and nitrate, respectively (5, 33).

The denitrification rate (R_{den}) was represented via a Michaelis-Menten-type equation (37, 40), taking into account limitation by NO_3^- and inhibition by O_2:

$$R_{den} = R_{max} \cdot \frac{[NO_3^-]}{[NO_3^-] + K_m} \cdot \frac{K_{O_2}}{[O_2] + K_{O_2}} \quad (3)$$

where the default values of K_m and the O_2 inhibition constant (K_{O_2}) were set at 250 μmol liter^{-1} (18) and 5 μmol liter^{-1} (23), respectively. R_{max} was initially assigned the value derived from the nitrate consumption rate measurements in the flowthrough reactor experiments and then optimized using the time-dependent N_2O profiles. Note that R_{max} and K_m are apparent kinetic parameters that depend on factors such as organic matter availability and community composition.

The NO_3^- and N_2O concentrations measured for the overlying water were used as upper boundary conditions, while zero-concentration gradients were used as lower boundaries. For the transient calculations, the measured ambient NO_3^- and N_2O profiles were used as the initial conditions. Pore water O_2 profiles depend on a multitude of reactions (41) and hence were not explicitly computed. Rather, the measured O_2 profiles were used in order to calculate the inhibition term in equation 3. The validity of this approach was confirmed by the time series O_2 microprofiles, which showed that there were no significant changes in the O_2 concentrations over the duration of the incubations (see below).

The depth distributions of N_2O production rates during the acetylene block experiments were estimated from the time series N_2O microprofiles by solving equation 2 for the rate, $R(x,t)$. The second-order spatial derivative in the diffusion term was approximated by the time-averaged change in slope of consecutively measured concentration profiles, whereas the partial derivative of concentration with respect to time was approximated as follows:

$$\left.\frac{\partial C}{\partial t}\right|_{t_{i+1/2}} \approx \frac{C^{t_{i+1}} - C^{t_i}}{t_{i+1} - t_i} \quad (4)$$

For simplicity, nonlocal exchange was ignored (i.e., $\alpha = 0$).

RESULTS

Sediment and pore water characteristics. The uppermost centimeters of sediment at Appels had high porosities and

Downloaded from http://aem.asm.org/ on December 8, 2020 at MAX-PLANCK-INSTITUT FUR

TABLE 1. Sediment properties

Depth (cm)	Organic C concn (%)	Molar organic C/N ratio	Mean grain size (μm)	Porosity (%)
0–1	1.6	12.3	106	80
1–2	2.5	12.1	67	76
2–3	2.7	13.6	37	66

organic carbon contents on the order of 1.5 to 3% (wt/wt) (Table 1). At both sampling times, August 2001 and August 2002, O_2 penetrated approximately 2 to 3 mm below the SWI (Fig. 1). High NO_3^- concentrations were found in the river water at the site (around 300 μmol liter^{-1} and 200 μmol liter^{-1} in August 2001 and August 2002, respectively). The ambient N_2O concentrations were always below the detection limit of the N_2O microsensor (~1 μmol liter^{-1} N_2O). The most probable numbers showed that microorganisms capable of denitrification were present at high densities (~10^8 cells cm^{-3} wet sediment) at all depths investigated (0 to 3 cm).

Enhanced pore water transport. After 36 h, bromide penetrated to a depth of about 5 cm, and there was good reproducibility for the three replicate cores (Fig. 1A). To quantify pore water mixing in addition to molecular diffusion, the profiles were fitted to solutions of equation 2, taking into account the depletion of Br^- in the overlying water with time. Except for the topmost 1 cm of sediment, simulations assuming molecular diffusion only were in good agreement with the measurements, implying that there was no deep (≥1-cm) pore water irrigation. On a vertical scale smaller than that resolved by the bromide measurements, however, a mixed zone in the uppermost 0.75 mm (x_{irr}) was identified based on the distinct kink in the O_2 microprofiles at that depth (Fig. 1B). An average value for the nonlocal exchange coefficient of 55 h^{-1} was constrained by fitting the O_2 microprofiles with equation 1, assuming a steady state and a Michaelis-Menten kinetic formulation for the net rate of O_2 consumption. The affinity constant for O_2 was set at 10 μmol liter^{-1} (41), and the maximum O_2 consumption rate was estimated from $2\phi D_s(C_0 - C_L)/L^2$, where the O_2 penetration depth (L) corresponds to the depth at which the O_2 concentration drops to 1 μmol liter^{-1} (i.e., C_L = 1 μmol liter^{-1}) and ϕ is the porosity. A satisfactory match between measured and predicted O_2 profiles was obtained with α values in the range from 10 to 100 h^{-1} (Fig. 1B).

The very shallow mixed zone is unlikely to be due to the activity of benthic infauna, which at Appels is dominated by oligochaete worms (35). We believe that this zone reflects an experimental artifact caused by the stirring of the overlying water in the cores. Air sparging and stirring of the overlying water were carried out to avoid progressive chemical stratification and ultimate anoxia of the waters just above the sediment. This would have interfered with the establishment of a steady-state distribution of denitrification activity, hence compromising the interpretation of time series N_2O microprofiles. Enhanced pore water mixing in the upper 0.75 mm of the sediment was accounted for in the reactive-transport calculations by using the same α values for all solute species (55 h^{-1}).

FTR experiments. The maximum potential nitrate consumption rate obtained in the FTR experiments decreased from 585 nmol cm^{-3} h^{-1} in the first centimeter of the sediment (0 to 1 cm) to 320 and 225 nmol cm^{-3} h^{-1} in the two deeper intervals (1 to 2 and 2 to 3 cm, respectively). Because of the high rates of nitrate reduction, relatively high inflow NO_3^- concentrations were needed in the FTR experiments in order to recover measurable NO_3^- concentrations in the outflow. As a result of the high average nitrate concentrations in the reactors, the measured rates approached the maximum values, and the estimated R_{max} values were not very sensitive to the value assigned to K_m. In additional acetylene block FTR experiments with Appels sediment, 80 to 100% of the NO_3^- consumed was recovered as N_2O (18), implying that under the experimental

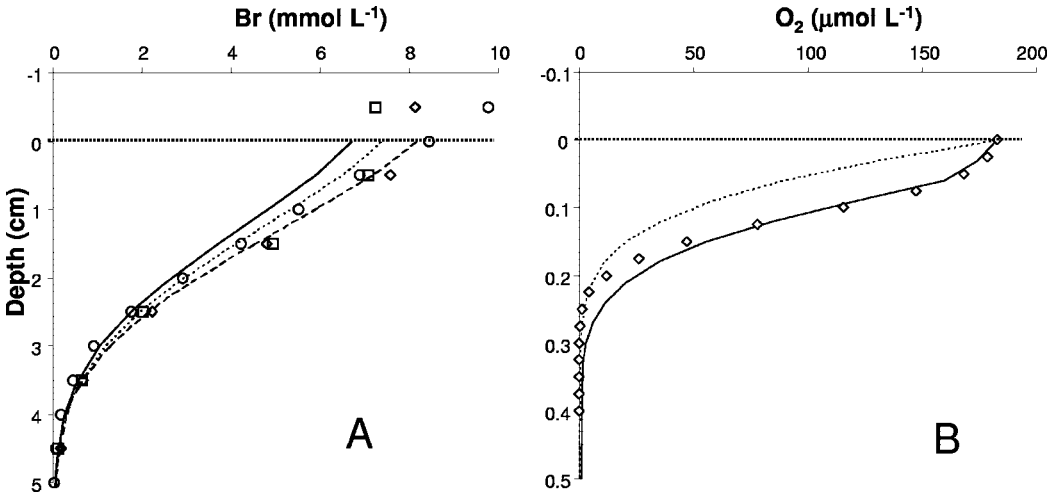

FIG. 1. Bromide (A) and oxygen (B) pore water profiles in sediment cores collected in August 2002 at Appels. Note the difference in the vertical scales. The three sets of symbols (measured data) and lines (model calculated) for bromide correspond to three replicate core incubations; the circles, diamonds, and squares correspond to the dotted, dashed, and solid lines, respectively. The calculated bromide profiles assume that there was no enhanced pore water mixing (α = 0). The dotted line in panel B corresponds to a model-predicted steady-state O_2 profile assuming that there was no enhanced mixing, whereas the solid line includes nonlocal pore water transport in the top 0. 75 mm with an α value of 55 h^{-1}. See the text for details.

Downloaded from http://aem.asm.org/ on December 8, 2020 at MAX-PLANCK-INSTITUT FUR

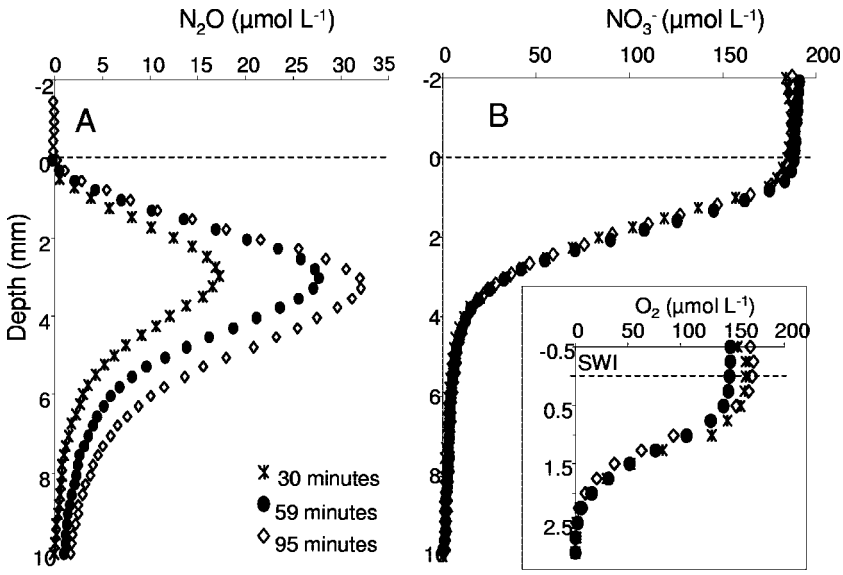

FIG. 2. Examples of microprofiles of N_2O (A), NO_3^- (B), and O_2 (inset) in an acetylene block core incubation experiment carried out in August 2002. The profiles were recorded 30, 59, and 95 min after addition of C_2H_2 to the overlying water and the pore waters via lateral injection ports.

conditions used, denitrification to N_2 is the dominant pathway of nitrate reduction.

Acetylene block core incubations. In sediment cores in which C_2H_2 was added to the overlying water, as well as injected laterally into the sediment, increasing pore water concentrations of N_2O occurred as a function of time. A selected number of N_2O depth profiles from a time series experiment carried out in August 2002 are shown in Fig. 2A. The profiles exhibited a distinct maximum at a depth of around 3 mm, with maximum concentrations of ~35 μmol liter^{-1} measured after 95 min. The maximum N_2O concentrations occurred below the depth where O_2 penetrated (Fig. 2). Oxygen and NO_3^- microprofiles determined alongside the N_2O profiles showed little change during the total time of the incubations (Fig. 2B). As was observed for the ambient O_2 microprofiles (Fig. 1B), the nitrate and O_2 profiles recorded during the C_2H_2 block experiments showed that there was a pronounced change in gradient at a depth of around 0.75 mm (Fig. 2B).

The rate profiles calculated at different times during the acetylene block experiments did not differ significantly over the time scale of the incubations (Fig. 3). The results showed that there was a narrow, 2- to 3-mm-thick layer of denitrification, located between the depths of penetration of O_2 and NO_3^- (Fig. 3). The denitrification activity peaked at depths of around 3 mm in both 2001 and 2002, and the maximum rates were in the range from 200 to 400 nmol N cm^{-3} h^{-1}.

The negative rates in the uppermost millimeters were due to the additional removal of N_2O by enhanced pore water transport (see above). When the negative rates were ignored, the integrated N_2O production rates in the sediment were on the order of 60 ± 12 nmol N cm^{-2} h^{-1} for August 2001 and 50 ± 8 nmol N cm^{-2} h^{-1} for August 2002. Note that because acetylene also blocks nitrification, these integrated N_2O production rates should have reflected only denitrification supported by NO_3^- uptake from the overlying water.

Addition of NO_3^- to the overlying water and sediment pore waters resulted in N_2O concentrations that were more than 1 order of magnitude higher than the values observed in the acetylene block incubations with no added NO_3^- (compare Fig. 2A and 4). The maximum concentrations also occurred deeper in the cores, indicating that NO_3^- added below the ambient nitrate penetration depth was actively used in denitrification. This observation agreed with the observed presence of

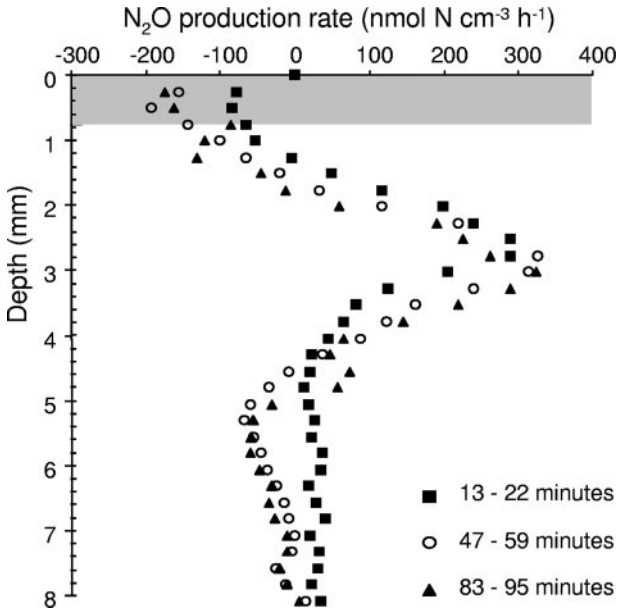

FIG. 3. N_2O production rates for a number of selected time intervals in the same acetylene block core incubation experiment as in Fig. 2. Each rate profile was derived using two successive N_2O profiles (measurement times are indicated), assuming that there was no enhanced pore water transport ($\alpha = 0$). The shading corresponds to the uppermost sediment layer which exhibits evidence of enhanced pore water transport. See the text for a complete discussion.

Downloaded from http://aem.asm.org/ on December 8, 2020 at MAX-PLANCK-INSTITUT FUR

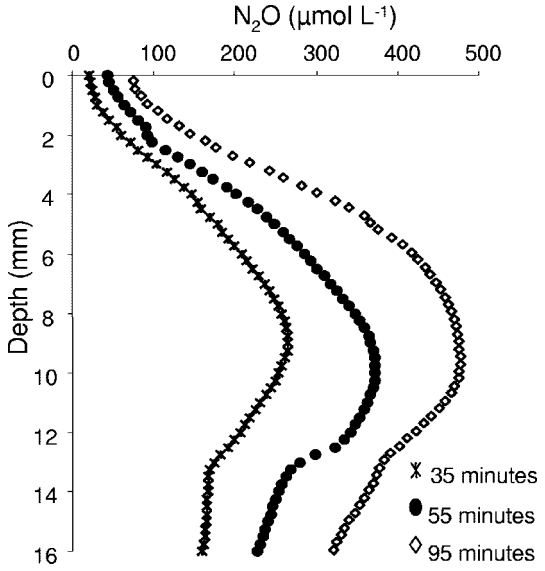

FIG. 4. Examples of N_2O profiles recorded during a core incubation experiment (August 2002) after simultaneous addition of C_2H_2 and NO_3^- to the overlying water and pore water. See the text for details.

denitrifying microorganisms several centimeters below the SWI, as well as the high potential nitrate reduction rates measured with the flowthrough reactors at depths below 1 cm.

Nitrate fluxes. The benthic NO_3^- uptake flux, obtained from the measured loss of nitrate from the overlying water in the unamended core incubations in August 2002, was 45 ± 14 nmol N cm^{-2} h^{-1}. Diffusive nitrate fluxes were also estimated from the linear portions of the depth profiles for NO_3^- concentrations below the zone of enhanced transport, according to the following equation:

$$F = -\phi D_s \frac{\Delta C}{\Delta x} \quad (5)$$

where the concentration gradient was evaluated below 0.75 mm. For the near-steady-state nitrate profiles measured during the acetylene block experiments with no added nitrate in August 2002 (Fig. 2B), equation 5 yielded downward nitrate fluxes into the zone of denitrification of 60 ± 15 nmol N cm^{-2} h^{-1}. The nitrate fluxes were thus the same order of magnitude as the integrated N_2O production rate in the August 2002 acetylene block core incubations with no added nitrate.

Reactive transport modeling. A baseline simulation of the August 2002 acetylene block experiment was carried out using the maximum potential nitrate reduction rate measured for the 0- to 1-cm sediment slice (R_{max} = 585 nmol cm^{-3} h^{-1}), the default nitrate half-saturation constant (K_m = 250 μM), and the default oxygen inhibition constant (K_{O_2} = 5 μmol $liter^{-1}$), plus the mixing parameters derived from the O_2 microprofiles (x_{irr} = 0.075 cm, α = 55 h^{-1}). Sensitivity analyses were then performed by multiplying or dividing the kinetic parameter values (R_{max}, K_m, and K_{O_2}) by 2. The results are summarized in Table 2, which also shows the model-predicted effect of the overlying water NO_3^- concentration on pore water N_2O production in the acetylene block core incubation experiment.

Additional forward reactive transport simulations were carried out to match the measured N_2O concentration buildup in the sediment, by fixing either K_m or R_{max} to the values derived from FTR experiments. When K_m was set at 250 μmol $liter^{-1}$, R_{max} had to be adjusted to 950 nmol cm^{-3} h^{-1} in order to reproduce the time series N_2O profiles (Fig. 5A). With this set of parameters, the calculated NO_3^- concentration profile closely resembled the measured profile (Fig. 5B). As observed, most denitrifying activity was predicted to be restricted to the 1.5- to 4-mm depth interval, although the modeled rates tended to be somewhat lower than the N_2O production rates estimated from the time series N_2O profiles (Fig. 6A). There was also a slight offset of about 0.5 mm between the calculated and observed depths at which the maximum N_2O concentration and production rate were reached.

An equally good fit to the observed values was obtained when we fixed R_{max} at 585 nmol cm^{-3} h^{-1} and reduced K_m to 100 μmol $liter^{-1}$ (results not shown). With both sets of K_m and R_{max} values, the depth-integrated steady-state rate of N_2O production calculated with the reactive transport model for August 2002 was 37 nmol N cm^{-2} h^{-1}. Irrespective of the actual K_m and R_{max} values used, the reactive transport simulations predicted that the NO_3^- concentration profiles should reach steady state shortly after C_2H_2 injection, while the buildup of N_2O in the pore waters should continue for several hours (Fig. 5A, inset). These predictions were consistent with the observations.

TABLE 2. Model sensitivity analyses: effects of the NO_3^- concentration in the overlying water and kinetic parameters (R_{max}, K_m, and K_{O_2}) on pore water N_2O buildup during simulated acetylene block core incubations[a]

$[NO_3^-]_{0LW}$ (μmol $liter^{-1}$)	R_{max} (nmol N cm^{-3} h^{-1})	K_m (μmol $liter^{-1}$)	K_{O_2} (μmol $liter^{-1}$)	$[N_2O]_{max}$ (μmol $liter^{-1}$)	Maximum N_2O production rate (nmol N cm^{-3} h^{-1})	Integrated N_2O production rate (nmol N cm^{-2} h^{-1})
188	585	250	5	19.6	135.0	28.7
188	585	125	5	26.7	193.1	35.4
188	585	500	5	12.9	86.6	20.5
188	293	250	5	11.8	76.9	19.0
188	1,170	250	5	28.7	224.8	37.8
188	585	250	2.5	18.9	134.9	27.0
188	585	250	10	20.3	139.5	30.9
94	585	250	5	12.0	76.4	15.8
376	585	250	5	32.2	222.1	50.4

[a] In the model simulations, the observed O_2 profile (Fig. 1 and 2) was imposed to account for inhibition of denitrification by O_2 (equation 3). The maximum N_2O concentrations ($[N_2O]_{max}$) and the N_2O production rates were calculated at 59 min. $[NO_3^-]_{0LW}$, NO_3^- concentration in the overlying water.

Downloaded from http://aem.asm.org/ on December 8, 2020 at MAX-PLANCK-INSTITUT FUR

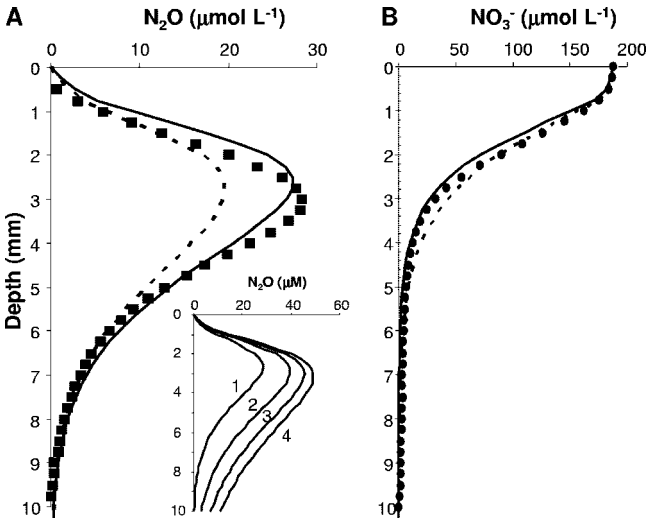

FIG. 5. Measured and model-predicted N_2O profiles (A) and measured and predicted NO_3^- profiles (B) after 59 min of incubation in an acetylene block core incubation experiment (August 2002) (see Fig. 2 and 3). The dashed lines are the modeled depth distributions obtained using a K_m value of 250 μmol liter^{-1} and an R_{max} value of 585 nmol cm^{-3} h^{-1}; the solid lines indicate modeled depth distributions obtained using a K_m value of 250 μmol liter^{-1} and an R_{max} value of 950 nmol cm^{-3} h^{-1}. In both simulations, the existence of a thin layer of enhanced pore water transport (x_{irr} = 0.75 mm) is assumed, with a constant exchange coefficient (α) of 55 h^{-1}. The inset shows the N_2O accumulation after 1, 2, 3, and 4 h. See the text for details.

DISCUSSION

Rate distribution and nitrate limitation. The results of the acetylene block experiments performed with cores with no added nitrate indicate that shortly (<15 min) after injection of C_2H_2, the depth profiles for pore water O_2 and NO_3^- reach steady state (Fig. 2B). The N_2O production rates derived from the time series N_2O microprofiles also imply that there was little variation in the depth distributions of denitrification activity during the experiments (Fig. 3).

Production of N_2O in the acetylene block experiments started at depths where pore water O_2 concentrations dropped below 50 μmol liter^{-1} and ended when pore water NO_3^- was exhausted (Fig. 2B and 3). As a result, denitrification was restricted to a sediment layer that was about 3 mm thick. The presence of such thin zones of denitrification has been reported previously for stream sediments (6), lake sediments (14, 15, 19), and estuarine sediments (4, 20).

Because of inhibition by O_2 in the uppermost 1 to 2 mm and, more importantly, because of the lack of NO_3^- at depths of >5 mm, only a small fraction of the denitrifying capacity of the sediment was utilized. This is shown in Fig. 6, where potential and in situ rates of denitrification are compared (Fig. 6A and B). It is also clearly evident from the instantaneous response of N_2O production to nitrate addition to the pore waters (Fig. 4) and is consistent with the presence of denitrifiers well below the depth of NO_3^- penetration (Fig. 6C).

The denitrification rates inferred from the acetylene block core incubations are lower than the maximum potential rate (R_{max}) measured for the 0- to 1-cm depth interval in the FTR experiments by a factor of about 2 (Fig. 6). Furthermore, the NO_3^- concentrations in the overlying water during the two sampling times fall in the range of nitrate half-saturation concentrations (K_m) derived from FTR experiments with estuarine sediments (200 to 600 μmol liter^{-1}) (18). Within the zone of maximum N_2O production (2 to 4 mm), the NO_3^- concentrations are well below the K_m.

Taken together, the results indicate that denitrification in the sediment is limited by nitrate. Consequently, the resident denitrifying community rapidly adjusts its level of activity to increased nitrate availability, as shown by the results of the NO_3^- addition core incubations (Fig. 4). The excess denitrifying capacity also implies that there is efficient utilization by the denitrifying community of nitrate produced by nitrification. In the mid-Scheldt Estuary downstream from Appels, up to 85% of total denitrification in intertidal sediments may be coupled to nitrification (21). The ability to rapidly respond to changes in the NO_3^- concentration should be a useful adaptation in intertidal estuarine sediments where the pore water composition and redox state can vary substantially on short time scales due to tidal flooding and irrigation by benthic infauna.

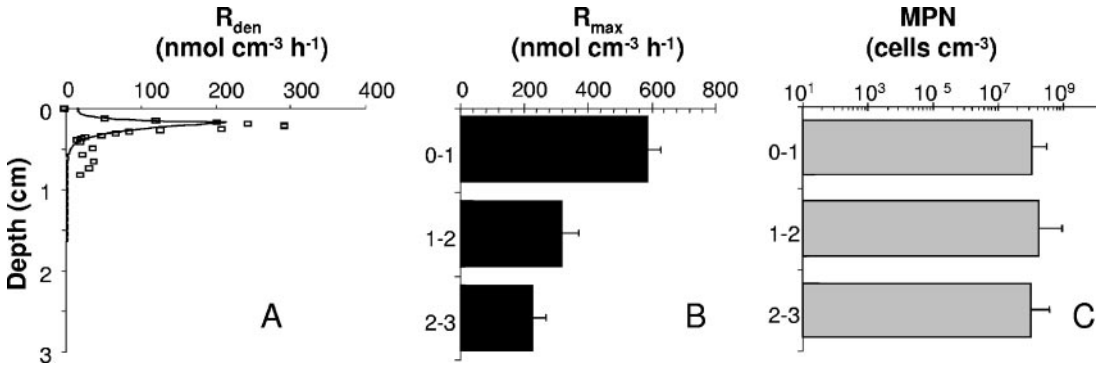

FIG. 6. In situ denitrification rates supported by nitrate uptake from the overlying water (A), maximum potential denitrification rates measured in flowthrough sediment reactors (B), and most probable numbers (MPN) of denitrifiers (C) in the top 3 cm of the sediment at Appels (August 2002). The solid line in panel A indicates the model-predicted in situ denitrification rate distribution in an acetylene block core incubation, obtained using a K_m value of 250 μmol liter^{-1}, an R_{max} value of 950 nmol cm^{-3} h^{-1}, an α value of 55 h^{-1}, and an x_{irr} value of 0.75 mm. The rectangles in panel A indicate the denitrification rates derived from the time series N_2O microprofiles (negative rates at the top were excluded for clarity).

Downloaded from http://aem.asm.org/ on December 8, 2020 at MAX-PLANCK-INSTITUT FUR

Microprofiling versus FTR experiments. Acetylene block and FTR experiments yield different, but complementary, kinetic information. The high-resolution denitrification rate distributions inferred from the N_2O microprofiles provide a precise determination of the in situ reaction zone (Fig. 3). In contrast, FTR experiments are designed to measure potential rates and parameterize predictive rate equations. Furthermore, the spatial resolutions of the two approaches are quite different, as the FTRs integrate the potential denitrifying activity over 1-cm depth intervals. However, as illustrated here, the differences between the two experimental approaches can be bridged through reactive transport modeling.

With the R_{max} value obtained in the 0- to 1-cm FTR experiment and the baseline K_m value, the model underpredicts the buildup of N_2O; the calculated maximum N_2O pore water concentrations are about one-third lower than the observed values (Table 2). Nonetheless, the forward reactive transport model calculations are able to forecast the general features of the acetylene block core incubation experiments. In particular, the model predicts that production of N_2O is restricted mainly to a narrow 2- to 3-mm zone. In addition, the model-calculated depth distribution of the N_2O production rate rapidly reaches steady state, while the pore water N_2O concentrations keep increasing for several hours.

Better agreement of the magnitudes of the concentrations and production rates of N_2O is obtained with the model by increasing R_{max} or decreasing K_m (Fig. 5). The significant decrease in the potential denitrification rate with depth (Table 1 and Fig. 6B) suggests that the average R_{max} for the 0- to 1-cm depth interval (585 nmol cm^{-3} h^{-1}) represents a lower limit for R_{max} in the zone of denitrification (0.1 to 0.5 cm). Furthermore, matching the N_2O profiles with an R_{max} value of 585 nmol cm^{-3} h^{-1} requires a K_m value (100 μM) that is at the extreme low end of the range obtained in a larger set of FTR experiments with Appels sediment (200 to 600 μM) (18). Therefore, by combining the various experimental and model-derived constraints, our best estimates for the ranges of the kinetic parameters in equation 3 are as follows: for K_m, 100 to 500 μM; and for R_{max}, 585 to 950 nmol cm^{-3} h^{-1}. Note that varying K_{O_2} by a factor of 2 has only a minor effect on the predicted N_2O concentrations and production rate (Table 2).

The K_m values derived from FTR experiments with natural estuarine sediments (18) are higher than the value determined for a pure culture of a nitrate-reducing bacterium, *Paracoccus denitrificans* (~10 μM) (26). They are, however, in line with the typically higher whole-sediment K_m values obtained in slurry or core incubation experiments (10, 17, 24, 27). The great variability of whole-sediment K_m values among different studies, which range from 10 to 600 μmol $liter^{-1}$, may reflect the great diversity of benthic communities of denitrifiers, which contain organisms exhibiting a wide range of nitrate affinities.

Biogeochemical implications. The integrated N_2O production rates determined in the acetylene block core incubations, the direct nitrate flux determinations, and the reactive transport modeling results all point to the high capacity for nitrate removal by the intertidal estuarine sediments in the upper Scheldt Estuary (21). High rates of benthic denitrification supported by nitrate uptake from the water column, similar to those at Appels (37 to 60 nmol N cm^{-2} h^{-1}), have been reported for nitrate-rich streams (~120 nmol N cm^{-2} h^{-1}) (7) and eutrophic estuaries in Denmark (40 to 140 nmol N cm^{-2} h^{-1}) (4, 20).

The experimentally calibrated reactive transport model provides further insight into the role of the kinetic parameters and the overlying water chemistry in denitrification activity in the sediments (Table 2). In particular, the benthic NO_3^- uptake and subsequent denitrification are very sensitive to the NO_3^- concentration in the overlying water. The water column NO_3^- concentrations in the freshwater part of the Scheldt Estuary exhibit large seasonal and interannual variations, with values ranging from a few micromoles per liter to 400 μmol $liter^{-1}$. For this range of overlying water NO_3^- concentrations, the model-predicted depth-integrated denitrification rates increase almost linearly with increasing NO_3^- concentrations at the water-sediment interface; that is, benthic nitrate uptake in the upper Scheldt Estuary should directly scale to the water column nitrate concentration.

For maximum potential denitrification rates up to about 1,000 nmol cm^{-3} h^{-1}, the model-calculated integrated rate of denitrification increases with increasing R_{max} (Table 2). At even greater values of R_{max}, however, the depth-integrated denitrification rate asymptotically approaches a maximum value (results not shown), reflecting the increasing rate-limiting effect of physical transport of nitrate from the water column to the zone of denitrification. Thus, a benthic denitrifying community exhibiting a potential metabolic capacity much lower than that inferred here from the combined experimental and modeling results (R_{max} range, 585 to 950 nmol cm^{-3} h^{-1}) would underutilize the high NO_3^- concentrations in the Scheldt River water, whereas a community with a much higher R_{max} would be only marginally more efficient in removing NO_3^- from the water column.

Although estuarine sediments are recognized as a sink for reactive nitrogen (3, 34), the role of benthic denitrification is often ignored in estuarine nitrogen models. For example, Regnier and Steefel (29) considered only water column denitrification in their non-steady-state N model of the Scheldt Estuary. The average values for the river discharge (30 m^3 s^{-1}) and dissolved inorganic N concentration (600 μmol $liter^{-1}$) yield a daily input of reactive dissolved inorganic nitrogen (NH_4^+ plus NO_3^-) to the upper Scheldt Estuary of around 22 tons N during the summer months. Multiplying the benthic nitrate uptake obtained in this study (~60 nmol cm^{-2} h^{-1}) by the surface area of freshwater tidal sediments (12.2×10^6 m^2) (P. Regnier, personal communication) yields a daily benthic uptake of about 2.5 tons of NO_3-N in the upper estuary alone. Although this is a very rough estimate, it indicates that sediments may be responsible for the removal of a considerable fraction of the reactive inorganic N entering the estuary.

ACKNOWLEDGMENTS

We thank Pieter Kleingeld, Debby Los, and Rick Canavan for field and laboratory assistance, Gaby Eickert and Ines Schröder for preparing the NO_3^- sensors, Jeffrey Abell and Caroline Slomp for comments on an earlier draft, and Parisa Jourabchi and Pierre Regnier for contributions to the modeling tools used in this study. The constructive comments of three journal reviewers helped improve the manuscript. The Netherlands Institute of Ecology in Yerseke (NIOO-CEMO) kindly provided logistical support.

This study was supported by the Netherlands Organisation for Scientific Research (NWO; Pioneer and Veni Programmes).

Downloaded from http://aem.asm.org/ on December 8, 2020 at MAX-PLANCK-INSTITUT FUR

REFERENCES

1. **Aguilera, D. R., P. Jourabchi, C. Spiteri, and P. Regnier.** 2005. A knowledge-based reactive transport approach for the simulation of biogeochemical dynamics in Earth systems. Geochem. Geophys. Geosyst. **6:**Q07012. [Online.] doi:10.1029/2004GC000899.
2. **Berner, R. A.** 1980. Early diagenesis: a theoretical approach. Princeton University Press, Princeton, NJ.
3. **Billen, G., M. Somville, E. de Becker, and P. Servais.** 1985. A nitrogen budget of the Scheldt hydrographical basin. Neth. J. Sea Res. **19:**223–230.
4. **Binnerup, S. J., K. Jensen, N. P. Revsbech, M. H. Jensen, and J. Sorensen.** 1992. Denitrification, dissimilatory reduction of nitrate to ammonium, and nitrification in a bioturbated estuarine sediment as measured with ^{15}N and microsensor techniques. Appl. Environ. Microbiol. **58:**303–313.
5. **Boudreau, B. P.** 1997. Diagenetic models and their implementation. Springer, Berlin, Germany.
6. **Christensen, P. B., L. P. Nielsen, N. P. Revsbech, and J. Sorensen.** 1989. Microzonation of denitrification activity in stream sediments as studied with a combined oxygen and nitrous oxide microsensor. Appl. Environ. Microbiol. **55:**1234–1241.
7. **Christensen, P. B., L. P. Nielsen, J. Sorensen, and N. P. Revsbech.** 1990. Denitrification in nitrate-rich streams—diurnal and seasonal variation related to benthic oxygen metabolism. Limnol. Oceanogr. **35:**640–651.
8. **Crutzen, P. J.** 1981. Atmospheric chemical processes of the oxides of nitrogen including nitrous oxide, p. 17–44. *In* C. C. Delwiche (ed.), Denitrification, nitrification and atmospheric nitrous oxide. John Wiley, New York, NY.
9. **De Beer, D., and J. P. R. Sweerts.** 1989. Measurement of nitrate gradients with an ion-selective microelectrode. Anal. Chim. Acta **219:**351–356.
10. **Garcia-Ruiz, R., S. N. Pattinson, and B. A. Whitton.** 1998. Kinetic parameters of denitrification in a river continuum. Appl. Environ. Microbiol. **64:**2533–2538.
11. **Gundersen, J. K., N. B. Ramsing, and R. N. Glud.** 1998. Predicting the signal of O_2 microsensors from physical dimensions, temperature, salinity and O_2 concentration. Limnol. Oceanogr. **43:**1932–1937.
12. **Herbert, R. A.** 1999. Nitrogen cycling in coastal marine ecosystems. FEMS Microbiol. Rev. **23:**563–590.
13. **Hyacinthe, C., and P. Van Cappellen.** 2004. An authigenic iron phosphate phase in estuarine sediments: composition, formation and chemical reactivity. Mar. Chem. **91:**227–251.
14. **Jensen, K., N. P. Revsbech, and L. P. Nielsen.** 1993. Microscale distribution of nitrification activity in sediment determined with a shielded microsensor for nitrate. Appl. Environ. Microbiol. **59:**3287–3296.
15. **Jensen, K., N. P. Sloth, N. Risgaard-Petersen, S. Rysgaard, and N. P. Revsbech.** 1994. Estimation of nitrification and denitrification from microprofiles of oxygen and nitrate in model sediment systems. Appl. Environ. Microbiol. **60:**2094–2100.
16. **Joye, S. B.** 2002. Denitrification in marine sediments, p. 1010–1019. *In* G. Britton (ed.), The encyclopedia of environmental microbiology. Wiley Publishers, New York, NY.
17. **Joye, S. B., S. V. Smith, J. T. Hollibaugh, and H. W. Paerl.** 1996. Estimating denitrification rates in estuarine sediments: a comparison of stoichiometric and acetylene based methods. Biogeochemistry **33:**197–215.
18. **Laverman, A. M., P. Van Cappellen, D. van Rotterdam-Los, C. Pallud, and J. Abel.** 2006. Potential rates and pathways of microbial nitrate reduction in coastal sediments. FEMS Microbiol. Ecol. **58:**179–192.
19. **Lorenzen, J., L. H. Larsen, T. Kjaer, and N. P. Revsbech.** 1998. Biosensor determination of the microscale distribution of nitrate, nitrate assimilation, nitrification, and denitrification in a diatom-inhabited freshwater sediment. Appl. Environ. Microbiol. **64:**3264–3269.
20. **Meyer, R. L., T. Kjaer, and N. P. Revsbech.** 2001. Use of NOx- microsensors to estimate the activity of sediment nitrification and NOx- consumption along an estuarine salinity, nitrate, and light gradient. Aquat. Microb. Ecol. **26:**181–193.
21. **Middelburg, J. J., G. Klaver, J. Nieuwenhuize, and T. Vlug.** 1995. Carbon and nitrogen cycling in intertidal sediments near Doel, Scheldt estuary. Hydrobiologia **311:**57–69.
22. **Nielsen, L. P., P. B. Christensen, N. P. Revsbech, and J. Sorensen.** 1990. Denitrification and oxygen respiration in biofilms studied with a microsensor for nitrous-oxide and oxygen. Microb. Ecol. **19:**63–72.
23. **Oh, J., and J. Silverstein.** 1999. Oxygen inhibition of activated sludge denitrification. Water Res. **33:**1925–1937.
24. **Oremland, R. S., C. Umberger, C. W. Culbertsen, and R. L. Smith.** 1984. Denitrification in San Francisco Bay intertidal sediments. Appl. Environ. Microbiol. **47:**1106–1112.
25. **Pallud, C., and P. Van Cappellen.** 2006. Kinetics of microbial sulfate reduction in estuarine sediments. Geochim. Cosmochim. Acta **70:**1148–1162.
26. **Parsonage, D., A. Greenfield, and S. J. Ferguson.** 1985. The high affinity of *Paracoccus denitrificans* cells for nitrate as an electron acceptor. Biochim. Biophys. Acta **807:**81–95.
27. **Raymond, N., P. Bonin, and J. C. Bertrand.** 1992. Comparison of methods for measuring denitrifying activity in marine sediments from the western Mediterranean coast. Oceanol. Acta **15:**137–143.
28. **Regnier, P., J. P. O'Kane, C. I. Steefel, and P. Vanderborght.** 2002. Modeling complex multi-component reactive-transport systems: towards a simulation environment based on the concept of a Knowledge Base. Appl. Math. Model. **26:**913–927.
29. **Regnier, P., and C. I. Steefel.** 1999. A high resolution estimate of the inorganic nitrogen flux from the Scheldt estuary to the coastal North Sea during a nitrogen-limited algal bloom, spring 1995. Geochim. Cosmochim. Acta **63:**1359–1374.
30. **Revsbech, N. P.** 1989. Diffusion characteristics of microbial communities determined by use of oxygen microsensors. J. Microbiol. Methods **9:**111–122.
31. **Revsbech, N. P., L. P. Nielsen, P. B. Christensen, and J. Sorensen.** 1988. Combined oxygen and nitrous oxide microsensor for denitrification studies. Appl. Environ. Microbiol. **54:**2245–2249.
32. **Rysgaard, S., N. Risgaard-Petersen, L. P. Nielsen, and N. P. Revsbech.** 1993. Nitrification and denitrification in lake and estuarine sediments measured by the N^{15} dilution technique and isotope pairing. Appl. Environ. Microbiol. **59:**2093–2098.
33. **Schulz, H. D.** 2000. Quantification of early diagenesis: dissolved constituents in marine pore water, p. 85–128. *In* H. D. Schulz and M. Zabel (ed.), Marine geochemistry. Springer, Berlin, Germany.
34. **Seitzinger, S. P.** 1988. Denitrification in freshwater and coastal marine ecosystems: ecological and geochemical significance. Limnol. Oceanogr. **33:**702–724.
35. **Seys, J., M. Vincx, and P. Meire.** 1999. Spatial distribution of oligochaetes (Clitellata) in the tidal freshwater and brackish parts of the Schelde estuary (Belgium). Hydrobiologia **406:**119–132.
36. **Soetaert, K., and P. M. J. Herman.** 1995. Carbon flows in the Westerschelde estuary (the Netherlands) evaluated by means of an ecosystem model (Moses). Hydrobiologia **311:**247–266.
37. **Tiedje, J. M., A. J. Sextone, D. D. Myrold, and J. A. Robinson.** 1982. Denitrification: ecological niches, competition and survival. Antonie Leeuwenhoek **48:**569–583.
38. **Tiedje, J. M., S. Simkins, and P. M. Groffman.** 1989. Perspectives on measurement of denitrification in the field including recommended protocols for acetylene based methods. Plant Soil **115:**261–284.
39. **Turner, R. E.** 2002. Element ratios and aquatic food webs. Estuaries **25:**694–703.
40. **Van Cappellen, P., and J. F. Gaillard.** 1996. Biogeochemical dynamics in aquatic sediments, p. 335–376. *In* P. C. Lichtner, C. I. Steefel, and E. H. Oelkers (ed.), Reactive transport in porous media: general principles and application to geochemical processes, vol. 34. American Mineralogical Society, Washington, DC.
41. **Wang, Y. F., and P. Van Cappellen.** 1996. A multicomponent reactive transport model of early diagenesis: application to redox cycling in coastal marine sediments. Geochim. Cosmochim. Acta **60:**2993–3014.
42. **Wollast, R.** 1988. The Scheldt Estuary, p. 183–193. *In* W. Salomons, B. L. Bayne, E. K. Duursma, and U. Forstner (ed.), Pollution of the North Sea. An assessment. Springer, Berlin, Germany.

Downloaded from http://aem.asm.org/ on December 8, 2020 at MAX-PLANCK-INSTITUT FUR